energy&fuels

Article

POTASSIUM CATALYTIC EFFECT ON GASIFICATION REACTIONS OF COAL AND COAL/BIOMASS BLENDS UNDER OXY-COMBUSTION CONDITIONS. AN ISOTOPIC STUDY USING 13C18O2

Yuli Betancur, Astrid E. Sanchez, Agustín Bueno-López, and Diana Patricia Lopez

Energy Fuels, **Just Accepted Manuscript** • DOI: 10.1021/acs.energyfuels.7b03399 • Publication Date (Web): 01 Jan 2018

ACS Publications

Energy & Fuels is published by the American Chemical Society. 1155 Sixteenth Street N.W., Washington, DC 20036

POTASSIUM CATALYTIC EFFECT ON GASIFICATION REACTIONS OF COAL AND COAL/BIOMASS BLENDS UNDER OXY-COMBUSTION CONDITIONS. AN ISOTOPIC STUDY USING $^{13}C^{18}O_2$

Yuli Betancur[1], Astrid Sánchez[2], Agustín Bueno-López[3] and Diana López[1*]

[1]Química de Recursos Energéticos y Medio Ambiente, Instituto de Química, Facultad de Ciencias Exactas y Naturales, Universidad de Antioquia, UdeA - Colombia, Calle 70 No. 52-21, Medellín, Colombia, Tel. +57 4 2196613

[2]Escuela de Química, Universidad Nacional de Colombia - Sede Medellín, Calle 59A No. 63-20, Medellín, Colombia

[3]Departamento de Química Inorgánica, Universidad de Alicante, Carretera de San Vicente s/n, E03080, Alicante, España.

[*]Corresponding author.

Telephone: + 57 4 2196613

E mail: diana.lopez@udea.edu.co

KEYWORDS. oxy-combustion, K_2CO_3 impregnation, coal/biomass blends, gasification reactions, isotopic labelled gas ($^{13}C^{18}O_2$).

ABSTRACT. In the present study, 20 wt % K_2CO_3 was added to coal and coal/biomass blends in 20:80 wt % ratio and subsequently were heating-treated at 600 °C using CO_2 or N_2 atmospheres. The reactivity under oxy-combustion conditions (21 % O_2 + 79 % CO_2) was studied by thermogravimetry, and characterization of chars was carried out by N_2 adsorption, scanning electron microscopy, Raman and X-ray photoelectron spectroscopy. It was observed higher activation energy for impregnated coal/biomass blends compared to impregnated coal, likewise, for materials thermally treated with CO_2. It is demonstrated that CO_2 gasification takes place together with O_2 combustion under oxy-combustion conditions. Isotopic labelled $^{13}C^{18}O_2$ was used to confirm the participation of CO_2 gasification reactions at 450, 500, 550 and 600 °C in both catalyzed and uncatalyzed systems under O_2 + CO_2. The catalytic effect of potassium promotes CO_2 gasification, and highest CO ($^{12}C^{18}O$) desorption was obtained with impregnated samples. It is possible to suggest that CO_2 gasification reactions follow different reaction pathways in presence or absence of potassium. The catalytic gasification reaction proceeded preferentially through a molecular CO_2 ($^{13}C^{18}O_2$) adsorption route while the non-catalyzed systems advanced using a dissociative adsorption pathway.

INTRODUCTION. Co-processing of coal with biomass (C/B) in thermal processes has gained interest because it represents a cleaner way to obtain energy and contributes to the decreasing of fossil fuels dependence. Partial replacement of coal by biomass leads to differences in the morphological and structural characteristics and behavior of obtained chars on thermochemical

transformation processes such as pyrolysis, combustion and gasification, which are also involved during oxy-combustion processes. This technology has several advantages compared to conventional combustion such as efficiency, NOx emissions reduction and easy CO_2 separation from other exhaust gases. On the other hand, the presence of biomass improves the reactivity of the obtained char due to its higher oxygen, volatile matter and mineral content [1], that play an important role during the oxy-combustion process. Besides, biomass is considered neutral regarding to CO_2 emissions.

During oxy-combustion, N_2 from air is replaced by a highly concentrated CO_2 atmosphere [2-4]. In this way, taking into account the high partial pressure of CO_2, increased reactivity of chars and higher mineral content on biomass compared to coal, make necessary to take gasification reactions into consideration [5].

The influence of gasification reactions on the temperature profiles, burnout time and consumption rates during the oxy-combustion process have been studied by simulating the gas atmospheres employed in oxy-combustion process (O_2/CO_2) [6-8]. The obtained results revealed that char gasification by CO_2 should not be neglected under oxy-combustion process because of the accelerated carbon consumption when CO_2 is present. This can be attributed to the CO_2 ability to penetrate the particles during the process, thus CO_2 reacts uniformly throughout the char particle, leading to structural changes [8].

In particular, studies using C/B blends under oxy-combustion conditions have been focused on the evaluation of techno-economical details, pollutant emissions, as well as thermal characteristics such as ignition and burnout temperature [9-11]. However, information about the contribution of CO_2 on the gasification reaction is required.

Gasification by CO_2 during the oxy-combustion process has been explained by the morphological differences such as porosity and surface area variations between C/B blends compared to the characteristics of individual coal or biomass [10, 12, 13]. On the other hand, simulation results revealed that coal char combustion temperature decreases considerably when gasification reactions by CO_2 are not ignored [6]. Therefore, it is important to include these reactions to interpret experimental and simulation data of chars under oxy-combustion conditions.

The gasification process has been modified by the presence of alkali and alkaline earth metals which have catalytic effects over this process [13-15]. Several studies have found that gasification of coal, biomass and other carbonaceous materials are catalyzed by potassium, present in biomass. In the evaluation of catalytic effect, typically potassium is added in the form of potassium carbonate (K_2CO_3) [16-19].

Some studies have assumed that the K_2CO_3-catalyzed gasification can occur by a redox cycle mechanism [16, 20, 21], in the first stage potassium ion is reduced by carbon to zero oxidation state and then, an oxygen atom from CO_2 oxidizes the potassium. The proposed reactions for CO_2 gasification are illustrated in equations (1)–(3) [22-24].

$$K_2CO_3 + \underline{C} \leftrightarrow 2K + \underline{C}O + CO_2 \qquad (1)$$

$$2K + CO_2 \rightarrow K_2O + CO \qquad (2)$$

$$K_2O + CO_2 \rightarrow K_2CO_3 \qquad (3)$$

Despite of numerous studies dedicated to investigate catalyzed gasification, there is a controversy about the interaction between carbon and catalyst. Particularly, regarding the surface intermediates of potassium involved during CO_2 gasification process, including: K, K_2O, K_2O_2, K_2CO_3, complexes such as $-CO_2K$, K–O–C, –CK and clusters [20, 25].

On the other hand, although the catalytic effect of minerals on the co-processing of coal and biomass has been demonstrated [14], the interactions between coal (C), coal/biomass (C/B) chars and potassium during oxy-combustion process need to be widely studied. Besides, it is important to clarify the effect of pre-treatment atmosphere in terms of reactivity, structural and morphological changes in nascent chars.

The aim of the present work is to determine the effect of CO_2 (balance gas) and potassium in the oxy-combustion process. The presence of gasification reactions was evaluated using coal and coal-biomass samples impregnated with K_2CO_3 and treated with N_2 or CO_2 atmospheres. The effect of gasification by CO_2 was studied using an isotopic labelled gas ($^{13}C^{18}O_2$) in order to differentiate the CO formed by the oxidation of an active site by oxygen ($^{16}O_2$) or the oxidation reactions in gas phase: ($^{13}C^{16}O$, $^{12}C^{16}O$) from carbon monoxide ($^{12}C^{18}O$) coming from reactions with the oxygen in the isotopic labelled gas ($^{13}C^{18}O_2$), which indicates its participation in gasification reactions during the oxy-combustion process.

EXPERIMENTAL METHODOLOGY

Samples preparation. A sub-bituminous coal and a lignocellulosic biomass residue from *Acacia mangium* (both acquired from Antioquia, Colombia), were used as raw materials and are referred as C and B, respectively. Coal and biomass were oven-dried at 110 °C for 24 h; subsequently the materials were grounded and sieved into particle sizes between 400 μm – 600 μm. With the aim to evaluate the potassium catalytic effect on gasification reactions, 20 wt % K_2CO_3 (i.e., K_2CO_3 powder, Merck 99.0 %) was added to C and C/B (80:20 wt % ratio) by wet impregnation.

The C and C/B impregnated chars were obtained using CO_2 or N_2 atmospheres at 600 °C with a heating rate of 20 °C/min in a horizontal tube furnace. Once the temperature reached 600 °C, the

samples were iso-thermally treated during 30 min. The impregnated chars were labeled as CIK-CO_2, CIK-N_2, C/BIK–CO_2 and C/BIK–N_2. Temperature selection was defined by the thermal conversion of raw material. Above 600 °C conversion was almost 100 %.

Samples characterization and combustion experiments. Mineral composition was determined using a PANalytical X-ray fluorescence spectrometer (XRF), proximate analysis was carried out by means of standard method ASTM D3172 employing a thermogravimetric balance (SDT Q600-TA Instruments).

Morphological and structural information for the impregnated chars were obtained by JEOL JSM-6490LV scanning electron microscopy (SEM). Raman spectroscopy analysis was achieved using a Jasco NRS-5100 spectrometer and X-ray photoelectron spectroscopy (XPS) was performed with a K-Alpha Thermo-Scientific spectrometer. High heating value (HHV) was determined by an oxygen bomb calorimeter using the standard method ASTM D5865. The specific surface areas for non-impregnated C, B, and C/B chars were obtained by N_2 adsorption at -196 °C with the Brunauer-Emmett-Teller (BET) model. The pore volumes were determined by means of N_2 adsorption at -196 °C and CO_2 adsorption at 0 °C with the Dubinin-Radushkevich (DR) model using an Autosorb-6B, from Quantachrome.

Oxy-combustion reactivity tests were carried out in a thermogravimetric analyzer (SDT Q600-TA Instruments) following the same methodology reported in a previous work [26].

Isotopic experiments. To obtain information about the gasification reactions involved during oxy-combustion conditions (O_2/CO_2), pulse experiments using isotopic labelled gases were performed. The isotopic labelled gas ($^{13}C^{18}O_2$; 95 % ^{13}C, 99 % $^{18}O_2$) was purchased from Sigma

Aldrich and $^{16}O_2$ (99.999 %) was provided by Abelló-Linde. Experiments were carried out in a quartz fixed bed microreactor with an internal diameter of 5 mm using 150 mg of impregnated samples (CIK and C/BIK). The samples were heated in inert gas (helium) with flow rate of 10 mL/min, and was switched to $^{16}O_2$ (10 mL/min) when the desired temperature was reached. 100 µL of $^{13}C^{18}O_2$ were pulsed at a pressure 5 psi and injected at different temperatures (450, 500, 550 and 600 °C) and three equivalent pulses were fed at each temperature.

RESULTS AND DISCUSSION

Surface area and morphological characteristics

Table 1 presents the ash composition, proximate analysis and higher heating value for raw materials (coal and biomass) obtained by XRF, TGA and calorimetry, respectively. It is important to highlight the higher content of catalytic species in biomass (species Ca and K), since their presence in the oxy-combustion process can favor the thermochemical transformation processes. However, the lower biomass calorific value and high volatile matter compared to coal indicate that the obtained energy, when biomass is burned alone is not enough compared with that obtained by coal combustion. Therefore, co-firing biomass with coal is an alternative to keep on the calorific value while mitigates CO_2 emissions.

It is important to note that, the impregnation process was quite effective since the obtained values of K-loaded, determined by atomic absorption spectrometry, were very close to those obtained from the stoichiometric ratio of K in K_2CO_3 (11 wt %). For example, for C/BIK chars obtained under N_2 and CO_2 treatment, the obtained values were 11.8 wt % and 10.9 wt %, respectively.

Table 1. Ash composition, calorific value and proximate analysis for raw materials

Figure 1 shows SEM and EDS mapping images for impregnated materials. It is observed that independently of the pre-treatment atmosphere (N_2 or CO_2), potassium was dispersed homogeneously over C and C/B chars, which is important because during the oxy-combustion process the potassium retained on chars acts as catalyst for the combustion and gasification processes [27], reducing the gasification temperature.

Figure 1. SEM-EDS mapping images of CIK and C/BIK chars obtained using N_2 or CO_2 at 600 °C

Table 2 indicates surface areas and pore volumes obtained for non-impregnated C, B, and C/B chars. The data for B-N_2 and C-N_2 are not shown because they are below the range of detection provided by the equipment. As can be seen in Table 2, there is a considerable increase in surface area for CO_2-chars compared with N_2-chars, especially in char blends. In addition, the nature of these materials after thermal treatment in both evaluated atmospheres was essentially microporous [26]. Thus, the spread of the catalyst throughout the surface of C and C/B chars can lead to the blocking of gases entrance into the micropores [23]. As a result, the significant decrease of the surface area does not allow the reliable BET surface values.

Table 2. BET surface and pore structure of non-impregnated chars

SEM micrographs in Figure 2 (a, b) show the CIK-N_2 and CIK-CO_2 images respectively. It is possible to appreciate a different surface conversion in both atmospheres, which suggests an important role of the pre-treatment conditions on the morphological and structural characteristics

of the chars. Therefore, these modifications have a direct influence on the reactivity during oxy-combustion.

Figure 2. SEM images of CIK and C/BIK chars obtained under N_2 (a, c, d) and CO_2 (b, e, f) at 600 °C

CIK-N_2 exhibits a smoother surface, while CIK-CO_2 shows a more heterogeneous structure with agglomerates formation on surface that can be a consequence of the high reactivity of the CO_2 atmosphere compared to the N_2 atmosphere [28], which implies that secondary reactions and recondensation products may be promoted under this atmosphere.

Regarding to the micrographs for the C/BIK chars in both evaluated atmospheres (Figure 2 (c-f)), biomass in blends (d, f) showed a higher cavities formation under both devolatilization atmospheres compared to coal that only exhibits cavities formation with CO_2 thermal treatment. These differences suggest that, the presence of biomass could induce physical changes on coal surface during the thermochemical transformation when CO_2 is used. This fact suggests an important effect of biomass on gasification reactions because the access and diffusion of reaction gases in the oxy-combustion process could be improved.

Raman Analysis

Raman spectra for CIK and C/BIK obtained under N_2 and CO_2 atmospheres were recorded. Only the results for CIK and C/BIK under CO_2 atmosphere are showed, since spectra with N_2 atmosphere did not differ considerably. The results of deconvolution and fitting curves are shown in Figure 3. All samples exhibit the characteristic D and G bands around 1340 cm^{-1} and 1605 cm^{-}

[1] respectively, which are typically found in carbonaceous materials [29, 30]. In this study, in order to visualize the possible changes in the carbonaceous structure, four contributions were identified in the 800-2000 cm^{-1} Raman shift range after deconvolution using Lorentzian functions, which are labelled as D_1, D_3, D_4 and G.

Figure 3. Raman spectra of CIK and C/BIK chars obtained under CO_2 atmosphere at 600 °C. Experimental data (-) and total fitted curve (---)

The D_1 band located around 1335 cm^{-1} corresponds to highly disordered carbonaceous material composed of carbon-carbon bonds in aromatic ring structures [30-32]. The D_3 band at 1500 cm^{-1} was assigned to methylene or methyl groups, amorphous carbon structures and smaller aromatics with 3–5 fused rings [32-34]. The D_4 band around 1200 cm^{-1} refers to aromatic-alkyl carbon bonds, aromatic/aliphatic ethers, C-H on aromatic rings and also it has been proposed as an indicator of active sites on carbons [35-38] and finally, the G band located around 1590 cm^{-1} was assigned to the graphitic component of carbonaceous materials [30].

Figure 4 shows the changes in the relative areas of D_i bands respect to G band (variation of the area ratio (A_{Di}/A_G)) as a function of the impregnated carbonaceous materials devolatilized with N_2 or CO_2. According with the A_{D1}/A_G ratio, CIK was not susceptible to changes with atmosphere modifications, but the addition of potassium on C/B blend (C/BIK), using CO_2, decreased the A_{D1}/A_G ratio, indicating an increment of condensation from aromatic rings. It is not necessarily associated with the graphitization degree, since it may have high condensation but as amorphous carbon.

The disordered structure leads to defects such as corners, edges or dislocations, indicating that C/BIK samples will be more active in gasification reactions.

The most significant differences between impregnated chars of C and C/B are shown in A_{D3}/A_G ratio. Although both materials exhibited the same trend toward the reduction of A_{D3}/A_G ratio when CO_2 was used, the decrease for C/BIK was more evident. This behavior suggests that the presence of potassium during the thermal process accelerates the cracking degree of the amorphous carbon fraction; therefore, the graphitization signal diminishes considerably. These results are in agreement with our previous work [26].

The explanation for this behavior is based on the higher number of potassium species in the C/B blend, due to the impregnation and the inherent amount from each individual material. It could favor the formation of K-C intercalated structures, since the alkali metal produced by the carbothermic reduction of K_2CO_3 (Equation 1) could attack a carbon atom and as a result of a charge transfer effect, the C-C bonds in chars suffer a weakening, thus favoring gasification with the CO_2 [17].

Figure 4. A_{Dx}/A_G ratio of the band peak areas of CIK and C/BIK chars prepared from CO_2 and N_2 atmosphere at 600 °C

However, it is important to consider that the decrease in the A_{D4}/A_G ratio for both samples with CO_2 treatment suggests that there are less active sites on the material surface, which can be associated to the smaller amount of intermediate potassium species formed under this atmosphere or active sites on char are more susceptible to react when CO_2 is used. These facts can explain the decrease in the reactivity of CO_2-chars during the oxy-combustion process.

XPS characterization

The alkali metallic species retained in carbonaceous materials are important during thermochemical processes because their influence on char reactivity [39]. In order to investigate the changes on the surface groups by the presence of potassium in coal and coal/biomass blends obtained under N_2 or CO_2 atmosphere, the XPS technique was used.

Table 3 shows the ratio of atomic surface composition measured by XPS. For all chars, the main composition was associated with C, K and O species. The overall balance was achieved with minority species of Ca, N, and Na.

Table 3. XPS-measured atomic surface composition in impregnated chars at 600 °C

The obtained differences in the composition of these chars for the evaluated atmospheres are illustrated in Figure 5. There is a more pronounced trend towards the decrease of C species and the K and O species increase when biomass is present during the thermochemical transformation process.

Particularly, the lower C1s proportion of C/BIK chars compared with CIK chars could be explained mainly by the higher CO_2 generation in the C/B mixture, since, as indicated in equation (4), the higher oxygen content in biomass compared to coal, can increase CO_2 production. Thus, CO_2 during the thermochemical process can participate in gasification of char such as Boudoard reaction (equation (5)), decreasing the amount of C-C bonds in both N_2 and CO_2 atmospheres when using C/BIK in comparison to CIK chars (11 % and 8 %, respectively).

$$C + O_2 \rightarrow CO_2 \qquad (4)$$

$$C + CO_2 \rightarrow 2\,CO \qquad (5)$$

Figure 5. Comparative composition of the C1s, K2p and O1s species in the CIK and C/BIK chars obtained under N_2 and CO_2 atmospheres

On the other hand, it is important to note that, the higher content of K and O species on C/BIK chars surface compared to the CIK chars is associated with the higher amount of these two species in biomass. The differences for the K2p and O1s signals between C/BIK and CIK chars under N_2 and CO_2 atmospheres are in agreement with the enhanced reduction of K_2CO_3 to activation of intermediate species suggested when using an atmosphere of N_2 compared to CO_2 [20], which is according with the obtained results for the A_{D4}/A_G ratio in the Raman analysis.

It is necessary to clarify that the inhibition of K_2CO_3 reduction over carbon surface might be hindered by the CO_2 atmosphere, because once the K_2CO_3 is reduced (i.e., releasing of CO), oxygen from CO_2 oxidizes the catalyst again [20].

In contrast, in a N_2 atmosphere, the carbon on char surface may be strongly bonded to the negatively charged oxygen atoms (from the carbonate) weakening the single bonds to carbon from the carbonate, which are finally broken during the thermal process. Thus, a further reaction between the oxygen from K-O produced in the previous step with the surface carbon, leads to the CO generation leaving a reduced potassium species, with an unknown stoichiometry as has been previously suggested [20].

Spectra for C1s, K2p and O1s of CIK and C/BIK chars under both reaction atmospheres were obtained. Only C/BIK spectrum is shown in Figure 6 as an example, due to the similarity

between peaks in CIK samples. Spectra deconvolution was performed employing three peaks for C1s, two peaks for K2p and three peaks for O1s in each atmosphere.

As indicated in Table 4, the three peaks regarding to C1s spectrum with binding energies of 284.6, 285.8 and 288.8 eV were assigned to C-C, C=O species of quinone, carbonyl groups and O-C=O groups of lactones and esters, respectively [24, 40, 41]. Besides 288.8 eV has been assigned to carbonates.

Figure 6. XPS spectra of C1s, K2p and O1s of C/BIK char using CO_2 (a-b) and N_2 (c-d)

As can be seen in Figure 6 (a) and (c), a considerable reduction in C−C species associate to C1s (peak 1) at binding energies of 284.6 eV was obtained under N_2 treatment. Besides, as indicated in Table 4 for C1s, the mentioned species decreased 11.9 % and 12.9 % for C/BIK and CIK, respectively, when atmosphere is changed from CO_2 to N_2. The bands at higher binding energies (292.6 eV and 295.3 eV; peaks 4 and 5) correspond to the electronic transitions from the $2p_{3/2}$ and $2p_{1/2}$ orbitals of potassium, respectively [42, 43]. It can be noted that total content of C=O and O-C=O species (peaks 2 and 3 in Figure 6 (a, c) and Table 4) decreased under a N_2 atmosphere, where K is present in a higher amount. This information indicates that both the atmosphere and the potassium presence could have important practical implications in the gasification reactions under oxy-combustion process.

It is important to mention that the K $2p_{1/2}$ signal can be associated to K_2O or KOH species, in accordance with previous reports, and they would be the active species at temperatures lower than 650 °C [17, 44]. Thus, the lower values in the area of these species when CO_2 was used instead

of N_2 could be attributed to their low thermal stability and the preferential reaction of CO_2 with the active sites during the thermal process, as well as the inhibition of their reduction under this oxidant atmosphere, as previously reported [20].

Table 4. Areas of C1s and K2p species for impregnated chars under CO_2 and N_2

Finally, Table 5 presents the area values of O1s species for CIK and C/BIK chars under the evaluated atmospheres. Peak A at 531.6 eV is associated to both carbonyl and semiquinone groups. Peak B at 533.2 eV is assigned to quinones or oxygen by a double bond in lactones, and the signal for peak C at 534.9 eV corresponds mainly to the oxygen of ether functionality [45-47].

Considering that peaks A and B (Figure 5 (b, d) and Table 5) are the major species for all samples, and those oxygenated species with the presence of C1s signal (peak 3, Table 4) are attributed to potassium carbonate [48, 49], it is possible to suggest that K_2CO_3 may be the main species catalyzing the thermochemical transformation processes involved in the oxy-combustion when impregnated samples are used.

Table 5. Area of O1s species for impregnated chars under CO_2 and N_2

Reactivity of materials under oxy-combustion conditions

Oxy-combustion experiments were performed, and Figure 7 shows the comparative DTG (derivative thermogravimetric) curves for CIK and C/BIK chars prepared under N_2 and CO_2 atmospheres. It can be appreciated, for all chars, a different thermal behavior, which suggests the

presence of species with different reactivity. CIK CO_2, C/BIK N_2 and C/BIK CO_2 exhibited a small shoulder between 350 and 450 °C, while CIK N_2 showed two well differentiated peaks in this range. The impregnated chars obtained under N_2 atmosphere showed a higher reactivity compared to chars-CO_2. Differences in reactivity could be associated mainly with the higher presence of active intermediate species of potassium on char surface, favored by using the N_2 atmosphere in the thermal process [20], which is consistent with the Raman and XPS results.

Thereby, as shown in Figure 7 and Table 6, the most reactive system was CIK-N_2 which showed the formation of species with higher reactivity during the first devolatilization stage (300 °C - 420 °C). The higher amount of active species on char surface could facilitate the CO_2 chemisorption during the oxy-combustion process, leading to the breaking of C-C bonds, which explains the decrease in the activation energy.

Particularly, the lower reactivity of C/BIK chars can be attributed to the increased CO_2 production during thermochemical transformation, favored by the higher oxygen content in biomass. Therefore, an inhibition of K_2CO_3 reduction to more active intermediates in C/BIK materials under both pre-treatment atmospheres (N_2 and CO_2) could occur increasing the activation energy values during the oxy-combustion process as it was observed.

Figure 7. Oxy-combustion experiments performed with CIK and C/BIK prepared under N_2 and CO_2 at 600 °C. Oxy-combustion conditions: 21% O_2 + 79% CO_2 gas flow and heating rate of 5 °C/min

Table 6. Activation energy for CIK and C/BIK chars under oxy-combustion conditions

The activation energies showed in Table 6, were determined using the non-isothermal thermogravimetric method and treating the obtained data under the mathematical model of the maximum speed, as indicated in our previous study [26]. Before determination of kinetic values, tests for avoiding diffusional effects were evaluated. Sample amount and particle size were determined after performing different analyzes varying these parameters, guaranteeing there is no diffusional restriction.

The reactivity of chars toward gasification process strongly depends on the distribution of surface functional groups. To show that dependence, in Figure 8, a correlation between reactivity and changes on the D_4 and G bands (A_{D4}/A_G) ratio of Raman were plotted for the CIK and C/BIK chars obtained under N_2 and CO_2 atmospheres.

Figure 8. Correlation between the activation energies and active sites on the material surface of the CIK and C/BIK obtained under N_2 and CO_2 at 600 °C

Considering independently the obtained results for CIK in both evaluated atmospheres (N_2 and CO_2) with those obtained for C/BIK chars (Figure 8), it is possible to appreciate that CIK was the more reactive system because it showed lower activation energy values and the higher A_{D4}/A_G ratio under each devolatilization atmospheres compared to C/BIK. However, both samples (CIK and C/BIK) showed a trend to lower activation energy values when N_2 was used in the thermal process instead of CO_2. It is related with the amount of active intermediate K species on char surface (higher presence when N_2 atmosphere is used), especially for CIK compared with C/BIK chars, given the CO_2 increase by the biomass presence that inhibits the formation of potassium species. Although different amount of active sites were obtained for each sample as a function of

pre-treatment atmosphere, it was possible to establish a direct correlation between the amount of active sites and the reactivity.

On the other hand, it is important to mention that the lower amount of active sites (lower A_{D4}/A_G ratio) when CO_2 is used, could also be associated with the consumption of those species by the CO_2, indicating possible gasification reactions.

Pulse experiments with isotopic labelled carbon dioxide ($^{13}C^{18}O_2$)

The reactions taking place under oxy-combustion condition were studied by mass spectrometry using non labelled O_2 ($^{16}O_2$) and labelled CO_2 ($^{13}C^{18}O_2$). Table 7 shows the monitored signals (m/z) with the associated species.

Table 7. Monitored masses after $^{16}O_2/^{13}C^{18}O_2$ pulses over CIK and C/BIK chars

Special attention was paid to the nature of the CO molecules to confirm the participation of oxygen from CO_2 in gasification reactions during oxy-combustion process of CIK and C/BIK chars.

Thus, $^{12}C^{16}O$ produced by oxidation of an active site by $^{16}O_2$ over chars is differentiated from CO coming from oxidation reactions in gas phase ($^{13}C^{16}O$, $^{13}C^{18}O$). Those species are differentiated from $^{12}C^{18}O$ coming from the carbon reaction with the oxygen present in the CO_2 balance gas (isotopically labelled, $^{13}C^{18}O_2$), which implies its participation in gasification reactions.

Quantification of carbon and oxygen in reaction products was performed taking into account the total amount of ^{13}C and ^{18}O, respectively. Thus, the percent obtained in each species after the

oxy-combustion process was calculated as shown below, taking as an example $^{13}C^{16}O_2$ and $^{12}C^{18}O_2$ for the carbon and oxygen balance, respectively:

$$\%\ \mathbf{^{13}C}^{16}O_2 = (({}^{13}C^{16}O_2) / ({}^{13}C^{16}O + {}^{13}C^{18}O + {}^{13}C^{16}O_2 + {}^{13}C^{16}O^{18}O + {}^{13}C^{18}O_2)) \times 100$$

$$\%\ {}^{12}C^{18}\mathbf{O_2} = ({}^{12}C^{18}O_2 \times 2) / ({}^{12}C^{18}O + {}^{13}C^{18}O + {}^{16}O^{18}O + ({}^{18}O_2 \times 2) + {}^{12}C^{16}O^{18}O + {}^{13}C^{16}O^{18}O + ({}^{12}C^{18}O_2 \times 2) + ({}^{13}C^{18}O_2 \times 2)) \times 100$$

Note that, ^{16}O atoms can come both from the solids (CIK, C/BIK or K_2CO_3 added) and from the $^{16}O_2$ supplied through external mass flow controllers to obtain the oxy-combustion gases mixture ($^{16}O_2/^{13}C^{18}O_2$), while ^{18}O atoms only come from the pulsed isotopic gas.

Figure 9 presents the MS profiles monitored for the ^{13}C (a) and ^{18}O (b) signals after $^{13}C^{18}O_2$ pulses using C/BIK CO_2 at 450 °C. The profiles for products including isotopically labelled oxygen (^{18}O) reveal that gasification reaction with CO_2 balance gas is occurring, since $^{12}C^{18}O$ product was obtained. It means that during oxy-combustion process, thermochemical transformation of coal or coal/biomass blends are not only a consequence of pyrolysis and combustion, but also gasification reactions are responsible for those conversions.

As can be seen in Figure 9 (a) the main products with ^{13}C were $^{13}C^{16}O_2$, $^{13}C^{16}O^{18}O$ and $^{13}C^{16}O$, while those with oxygen ^{18}O (Figure 9 (b)) were $^{12}C^{16}O^{18}O$, $^{13}C^{16}O^{18}O$ and $^{12}C^{18}O$. It is important to mention that isotopic recombination reactions play an important place during thermochemical process because, once the gasification occurs, reactions in the gas phase take place between the initial products with the oxygen (^{16}O) giving rise to the isotopic recombination products.

Figure 9. MS profiles monitored after $^{13}C^{18}O_2$ pulses to C/BIK CO_2 at 450 °C (a) ^{13}C carbon balance and (b) ^{18}O oxygen balance

Similar profiles were obtained for CIK chars under both atmospheres. Thus, in order to verify the potassium catalytic effect toward the $^{12}C^{18}O$ production, reaction products for coal without potassium impregnation obtained under N_2 and CO_2 atmospheres were monitored.

Previous reports indicate that the formation of different kind of oxygenated complexes on coal surface by the presence of catalyst is thermodynamically more favorable than the non- catalytic systems, and thus, catalyzed gasification reaction desorbs a higher CO amount compared with the absence of catalyst as the reaction proceeds [50].

However, results indicate that gasification is also occurring in the uncatalyzed reaction since the signal of $^{12}C^{18}O$ was also obtained for C chars. From Table 8 negligible differences in the percentages of $^{12}C^{18}O$ for impregnated and non-impregnated coal chars obtained under N_2 and CO_2 atmospheres and different temperatures were observed. The trend towards the higher amount of $^{12}C^{18}O$ desorbed for CIK-N_2 compared with CIK-CO_2 agrees with TGA and Raman results, since the higher evolution of reactive species during the first devolatilization stage for CIK-N_2 (Figure 7), as well as the higher A_{D4}/A_G ratio observed (Figure 8), suggest that the use of N_2 as a pre-treatment atmosphere led to more reactive systems.

Table 8. Percent of $^{12}C^{18}O$ evolution for impregnated and non-impregnated coal char, as a function of pre-treatment atmosphere and temperature

According to the obtained ratio for all monitored masses after injecting a $^{13}C^{18}O_2$ pulse over C, CIK and C/BIK chars, the most significant differences between the impregnated and non-impregnated chars are presented for the $^{12}C^{16}O^{18}O$, $^{13}C^{16}O_2$ and $^{13}C^{16}O^{18}O$ signals. For example, for C and CIK chars, the $^{12}C^{16}O^{18}O$ signal decreased 6 % when CIK-CO_2 was used instead of C-CO_2, while the use of CIK-N_2 instead of C-N_2 led to a 7 % increase. Regarding $^{13}C^{16}O_2$ signal, an increase of 12 % and 10 % was observed for CIK chars obtained under N_2 and CO_2 atmosphere, respectively, compared to the values for coal chars without impregnation.

Finally, the $^{13}C^{16}O^{18}O$ signal decreased 11 % in both evaluated atmospheres (N_2 and CO_2) when potassium is present in coal chars.

It is important to mention that, the slight variation on products distribution observed during the oxy-combustion process of chars allowed proposing the preferred route related to gasification reactions with CO_2 for catalyzed and non-catalyzed reactions.

Taking into account these results, we can propose catalyzed systems evolve through a molecular CO_2 ($^{13}C^{18}O_2$) adsorption route while the non-catalyzed systems proceed mainly using a dissociative adsorption pathway, as illustrated in Figures 10 and 11, respectively.

Figure 10. Molecular adsorption of $^{13}C^{18}O_2$ on two active sites, * represents the active sites associated with the K species presence

Figure 11. Dissociative adsorption of $^{13}C^{18}O_2$ on one active site

According with the proposed mechanisms and based on previous studies [51-53] that reported lower activation energies in gasification reactions of potassium catalyzed chars compared with

uncatalyzed systems, a fact that can be associated with two main reasons, including an increase in the active site density by the catalysts presence as well as the inhibition to graphitization and condensation of chars, increasing in both cases the gasification reactivity of chars. It is possible to argue that the first proposed route (Figure 10), which is the preferential pathway through the catalytic gasification reaction proceeded, correspond to the route that involves less activation energy, as is expected for catalyzed systems.

The obtained differences for the $^{13}C^{16}O_2$ and $^{13}C^{16}O^{18}O$ species when using the material with or without impregnation were determinant to understand which route prevails in the gasification process; its formation is a consequence of the recombination with ^{16}O used for the mixture of reaction ($\mathbf{^{16}O_2}$/$^{13}C^{18}O_2$).

On the other hand, the CO_2 ($^{13}C^{18}O_2$) dissociation forms one or two active sites over char surface liberating $^{12}C^{18}O$ thanks to the weakened C-C bonds. A homogeneous reaction between the gasification product ($^{12}C^{18}O$) and the $^{13}C^{16}O$ species with $^{16}O_2$ occurs giving rise to considerably higher amounts of $^{12}C^{16}O^{18}O$ and $^{13}C^{16}O^{18}O$ compared to the obtained ratio for the initial species produced.

CONCLUSIONS. Results indicated that thanks to the N_2 treatment, impregnated chars gave rise to the formation of a higher amount of active potassium species in comparison with the CO_2 atmosphere. The reason for this behavior can be explained by the favored reduction of K_2CO_3 in N_2 pre-treatment atmospheres. On the contrary, the prompt oxidation of reduced carbonate caused by the oxygen atoms coming from the CO_2 present in the pre-treatment atmosphere inhibits the formation of potassium species. Thus, during the oxy-combustion process, the

absence of such intermediates hinders the oxygen exchange from CO_2, the transfer to a free surface site and subsequent gasification during the oxy-combustion process.

Thereby, obtained chars under N_2 atmosphere showed a higher reactivity when used in the oxy-combustion. Comparison of the activation energies values between impregnated and non-impregnated materials confirm the catalytic effect of potassium species, since a reduction of 30 kJ/mol was observed when CIK-CO_2 is used instead of C-CO_2, while a more significant decrease was obtained for systems pre-treated with N_2 (44 kJ/mol) when CIK-N_2 was used rather than C-N_2. On the other hand, a higher amount of $^{12}C^{18}O$ was observed for impregnated chars, especially when N_2 is used, probably due to the higher proportion of surface potassium as indicated by XPS.

Although the activation energies for the C/BIK blends followed the same trend observed for CIK under both evaluated atmospheres, they were considerably higher. An increase of 51 kJ/mol when C/BIK was used instead of CIK in a CO_2 atmosphere and 30 kJ/mol for C/BIK-N_2 compared to CIK-N_2. It is important to emphasize that the higher CO_2 concentration in the C/B blends because of the higher oxygen concentration in biomass can explain the decrease in reactivity compared to the CIK system.

Finally, one of the main contributions of this study for CO_2 gasification reactions in the oxy-combustion process was associated with the possibility of suggesting a possible gasification pathway by having a catalyzed and uncatalyzed gasification reaction. Two reaction mechanisms were identified. The catalytic gasification reaction proceeds through a molecular CO_2 ($^{13}C^{18}O_2$) adsorption route while the non-catalyzed systems proceed mainly using a dissociative adsorption pathway.

ACKNOWLEDGEMENTS. The authors thank the "Departamento Administrativo de Ciencia, Tecnología e Innovación"- COLCIENCIAS (Administrative Department of Science, Technology and Innovation from Colombia) through the program "Research and innovation on advanced combustion in Industrial use", code N° 1115-543-31906 contract N° 0852-2012. The authors also thank the Universidad de Antioquia, Universidad Nacional de Colombia- Sede Medellín and Universidad de Alicante-Departamento de Química Inorgánica.

REFERENCES

1. Irfan, M. F.; Arami-Niya, A.; Chakrabarti, M. H.; Wan Daud, W. M. A.; Usman, M. R., Kinetics of gasification of coal, biomass and their blends in air (N_2/O_2) and different oxy-fuel (O_2/CO_2) atmospheres. *Energy* **2012,** 37, (1), 665-672.

2. Guedea, I.; Pallarès, D.; Díez, L. I.; Johnsson, F., Conversion of large coal particles under O_2/N_2 and O_2/CO_2 atmospheres—Experiments and modeling. *Fuel Processing Technology* **2013,** 112, 118-128.

3. Yuzbasi, N. S.; Selçuk, N., Air and oxy-fuel combustion behaviour of petcoke/lignite blends. *Fuel* **2012,** 92, (1), 137-144.

4. Bejarano, P. A.; Levendis, Y. A., Single-coal-particle combustion in O_2/N_2 and O_2/CO_2 environments. *Combustion and Flame* **2008,** 153, (1–2), 270-287.

5. Irfan, M. F.; Usman, M. R.; Kusakabe, K., Coal gasification in CO_2 atmosphere and its kinetics since 1948: A brief review. *Energy* **2011,** 36, (1), 12-40.

6. Hecht, E. S.; Shaddix, C. R.; Geier, M.; Molina, A.; Haynes, B. S., Effect of CO_2 and steam gasification reactions on the oxy-combustion of pulverized coal char. *Combustion and Flame* **2012,** 159, (11), 3437-3447.

7. Kim, D.; Choi, S.; Shaddix, C. R.; Geier, M., Effect of CO_2 gasification reaction on char particle combustion in oxy-fuel conditions. *Fuel* **2014,** 120, 130-140.

8. Singer, S.; Chen, L.; Ghoniem, A. F., The influence of gasification reactions on char consumption under oxy-combustion conditions: Effects of particle trajectory and conversion. *Proceedings of the Combustion Institute* **2013,** 34, (2), 3471-3478.

9. Cormos, C.-C., Oxy-combustion of coal, lignite and biomass: A techno-economic analysis for a large scale Carbon Capture and Storage (CCS) project in Romania. *Fuel* **2016,** 169, 50-57.

10. Riaza, J.; Gil, M. V.; Álvarez, L.; Pevida, C.; Pis, J. J.; Rubiera, F., Oxy-fuel combustion of coal and biomass blends. *Energy* **2012,** 41, (1), 429-435.

11. Smart, J. P.; Patel, R.; Riley, G. S., Oxy-fuel combustion of coal and biomass, the effect on radiative and convective heat transfer and burnout. *Combustion and Flame* **2010,** 157, (12), 2230-2240.

12. Gil, M. V.; Riaza, J.; Álvarez, L.; Pevida, C.; Rubiera, F., Biomass devolatilization at high temperature under N_2 and CO_2: Char morphology and reactivity. *Energy* **2015,** 91, 655-662.

13. Farrow, T. S.; Sun, C.; Snape, C. E., Impact of biomass char on coal char burn-out under air and oxy-fuel conditions. *Fuel* **2013,** 114, 128-134.

14. Masnadi, M. S.; Grace, J. R.; Bi, X. T.; Lim, C. J.; Ellis, N., From fossil fuels towards renewables: Inhibitory and catalytic effects on carbon thermochemical conversion during co-gasification of biomass with fossil fuels. *Applied Energy* **2015,** 140, 196-209.

15. Sadhwani, N.; Adhikari, S.; Eden, M. R.; Wang, Z.; Baker, R., Southern pines char gasification with CO_2—Kinetics and effect of alkali and alkaline earth metals. *Fuel Processing Technology* **2016,** 150, 64-70.

16. Zhang, J.; Zhang, R.; Bi, J., Effect of catalyst on coal char structure and its role in catalytic coal gasification. *Catalysis Communications* **2016,** 79, 1-5.

17. Wood, B. J.; Sancier, K. M., The Mechanism of the Catalytic Gasification of Coal Char: A Critical Review. *Catalysis Reviews* **1984,** 26, (2), 233-279.

18. Tsubouchi, N.; Nishio, M.; Mochizuki, Y., Role of nitrogen in pore development in activated carbon prepared by potassium carbonate activation of lignin. *Applied Surface Science* **2016,** 371, 301-306.

19. Islam, S.; Kopyscinski, J.; Liew, S. C.; Hill, J. M., Impact of K_2CO_3 catalyst loading on the CO_2-gasification of Genesse raw coal and low-ash product. *Powder Technology* **2016,** 290, 141-147.

20. Kopyscinski, J.; Rahman, M.; Gupta, R.; Mims, C. A.; Hill, J. M., K_2CO_3 catalyzed CO_2 gasification of ash-free coal. Interactions of the catalyst with carbon in N_2 and CO_2 atmosphere. *Fuel* **2014,** 117, Part B, 1181-1189.

21. F. Kapteijn, J. A. M., Kinetics of the potassium carbonate-catalyzed CO_2 gasification of activated carbon. *Fuel* **1983,** 62, 221–225.

22. Zhang, Y.; Zheng, Y.; Yang, M.; Song, Y., Effect of fuel origin on synergy during co-gasification of biomass and coal in CO_2. *Bioresource Technology* **2016,** 200, 789-794.

23. Sancier, B. J. W. a. K. M., The mechanism of the catalytic gasification of coal char: A critical review. *Catalysis reviews: Science and engineering* **1984,** 26, (2), 233-279.

24. Shankhamala Kundu, Y. W., Wei Xia, and Martin Muhler, Thermal Stability and Reducibility of Oxygen-Containing Functional Groups on Multiwalled Carbon Nanotube Surfaces: A Quantitative High-Resolution XPS and TPD/TPR Study. *Journal of Physical Chemistry C* **2008,** 112, 16869–16878.

25. Kim, Y.-K.; Hao, L.-f.; Park, J.-I.; Miyawaki, J.; Mochida, I.; Yoon, S.-H., Catalytic activity and activation mechanism of potassium carbonate supported on perovskite oxide for coal char combustion. *Fuel* **2012,** 94, 516-522.

26. Betancur, Y.; Sánchez, A.; Bueno-López, A.; López, D., Impact of Biomass and Main Biomass Components on Coal Reactivity under Oxy-Combustion Conditions—A Comparison of Physicochemical Char Properties Obtained under N_2 and CO_2 Atmospheres. *Energy & Fuels* **2017**.

27. Keown, D. M.; Hayashi, J.-i.; Li, C.-Z., Effects of volatile–char interactions on the volatilisation of alkali and alkaline earth metallic species during the pyrolysis of biomass. *Fuel* **2008,** 87, (7), 1187-1194.

28. Gil, M. V.; Riaza, J.; Álvarez, L.; Pevida, C.; Pis, J. J.; Rubiera, F., Oxy-fuel combustion kinetics and morphology of coal chars obtained in N_2 and CO_2 atmospheres in an entrained flow reactor. *Applied Energy* **2012,** 91, (1), 67-74.

29. Yan Wang, D. C. A., and Richard L. McCreery, Raman spectroscopy of carbon materials: Structural basis of observed spectra *Chemistry of Materials* **1990,** 2, 557-563.

30. Chabalala, V. P.; Wagner, N.; Potgieter-Vermaak, S., Investigation into the evolution of char structure using Raman spectroscopy in conjunction with coal petrography; Part 1. *Fuel Processing Technology* **2011,** 92, (4), 750-756.

31. Sadezky, A.; Muckenhuber, H.; Grothe, H.; Niessner, R.; Pöschl, U., Raman microspectroscopy of soot and related carbonaceous materials: Spectral analysis and structural information. *Carbon* **2005,** 43, (8), 1731-1742.

32. Guo X, T. H., Zhang S, Li CZ, Changes in char structure during the gasification of a victorian brown coal in steam and oxygen at 800 °C. *Energy & Fuels* **2008,** 22, 4034–4038.

33. Jawhari, T.; Roid, A.; Casado, J., Raman spectroscopic characterization of some commercially available carbon black materials. *Carbon* **1995,** 33, (11), 1561-1565.

34. Cuesta, A.; Dhamelincourt, P.; Laureyns, J.; Martínez-Alonso, A.; Tascón, J. M. D., Raman microprobe studies on carbon materials. *Carbon* **1994,** 32, (8), 1523-1532.

35. J. Schwan, S. U., V. Batori, and H. Ehrhardt, Raman spectroscopy on amorphous carbon films. *Journal of Applied Physics* **1996,** 80, 440–447.

36. T. Livneh, E. B.-z., P. Salatino, O. Senneca., Evolution of reactivity of highly porous chars from raman microscopy. *Combustion Science and Technology* **2000,** 153, 65–82.

37. D. Vien, B. C., G. Fateley, G. Grasselli., The handbook of infrared and Raman characteristic frequencies of organic molecules. San Diego, CA, USA: Academic Press,. **1991**, 476– 490.

38. R. Nemanich, J. G., G. Lucovsky, R. Shroder, Raman scattering characterization of carbon bonding in diamond and diamondlike thin films. *Journal of Vacuum Science & Technology A* **1988,** 6, 1783–1787.

39. Zhao, Y.; Feng, D.; Zhang, Y.; Huang, Y.; Sun, S., Effect of pyrolysis temperature on char structure and chemical speciation of alkali and alkaline earth metallic species in biochar. *Fuel Processing Technology* **2016,** 141, Part 1, 54-60.

40. Xia, W.; Yang, J., Effect of pre-wetting time on oxidized coal flotation. *Powder Technology* **2013,** 250, 63-66.

41. B. Wang, Y. P., S. Vink, Diagnosis of the surface chemistry effects on fine coalflotation using saline water. *Energy & Fuel* **2013,** 27, 4869–4874.

42. Courcot, D.; Gengembre, L.; Guelton, M.; Barbaux, Y.; Grzybowska, B., Effect of potassium on the surface potential of titania. *Journal of the Chemical Society, Faraday Transactions* **1994,** 90, (6), 895-898.

43. Freund, H. J.; Roberts, M. W., Surface chemistry of carbon dioxide. *Surface Science Reports* **1996,** 25, (8), 225-273.

44. Nzihou, A.; Stanmore, B.; Sharrock, P., A review of catalysts for the gasification of biomass char, with some reference to coal. *Energy* **2013,** 58, 305-317.

45. S. R. Kelemen, M. A., and M. L. Gorbaty, Characterization of Organically Bound Oxygen Forms in Lignites, Peats, and Pyrolyzed Peats by X-ray Photoelectron Spectroscopy (XPS) and Solid-State ^{13}C NMR Methods. *Energy & Fuels* **2002,** 16, 1450-1462.

46. Hao, S.; Wen, J.; Yu, X.; Chu, W., Effect of the surface oxygen groups on methane adsorption on coals. *Applied Surface Science* **2013,** 264, 433-442.

47. Desimoni, E.; Casella, G. I.; Salvi, A. M., XPS/XAES study of carbon fibres during thermal annealing under UHV conditions. *Carbon* **1992,** 30, (4), 521-526.

48. Shchukarev, A.; Korolkov, D., XPS Study of group IA carbonates. In *Open Chemistry*, 2004; Vol. 2, p 347.

49. Dwyer, D. J.; Hardenbergh, J. H., Catalytic reduction of carbon monoxide over potassium modified iron surfaces. *Applications of Surface Science* **1984,** 19, (1), 14-27.

50. Calderón, J. D. G., Efecto del calcio en los mecanismos de la reacción de gasificación de materiales carbonosos con CO_2. *Trabajo de Maestría. Facultad de Ciencias Exactas y Naturales. Posgrado en Ciencias Químicas, Medellín* **2012**.

51. Liu, Q.; Wang, S.; Luo, Z.; Cen, K., Catalysis Mechanism Study of Potassium Salts on Cellulose Pyrolysis by Using TGA-FTIR Analysis. *Journal of Chemical Engineering of Japan* **2008,** 41, (12), 1133-1142.

52. Nowakowski, D. J.; Jones, J. M.; Brydson, R. M. D.; Ross, A. B., Potassium catalysis in the pyrolysis behaviour of short rotation willow coppice. *Fuel* **2007,** 86, (15), 2389-2402.

53. Malekshahian, M.; Hill, J. M., Potassium catalyzed CO_2 gasification of petroleum coke at elevated pressures. *Fuel Processing Technology* **2013,** 113, 34-40.

Table 1. Ash composition, calorific value and proximate analysis for raw materials

Ash composition (wt %)	Sub-bituminous coal	*Acacia mangium*
Fe_2O_3	51.62	0.85
CaO	34.43	84.07
SO_3	9.09	1.33
TiO_2	2.22	-----
MgO	0.79	-----
WO_3	0.73	-----
NiO	0.71	-----
V_2O_5	0.42	-----
MnO	-----	2.26
SiO_2	-----	0.86
K_2O	-----	10.01
[a]Volatile matter (%)	42	64
[a]Fixed carbon (%)	56	33
[a]Ash (%)	2	3
*HHV (kJ/kg)	23004	20728

[a]Dry basis, *High-heating value

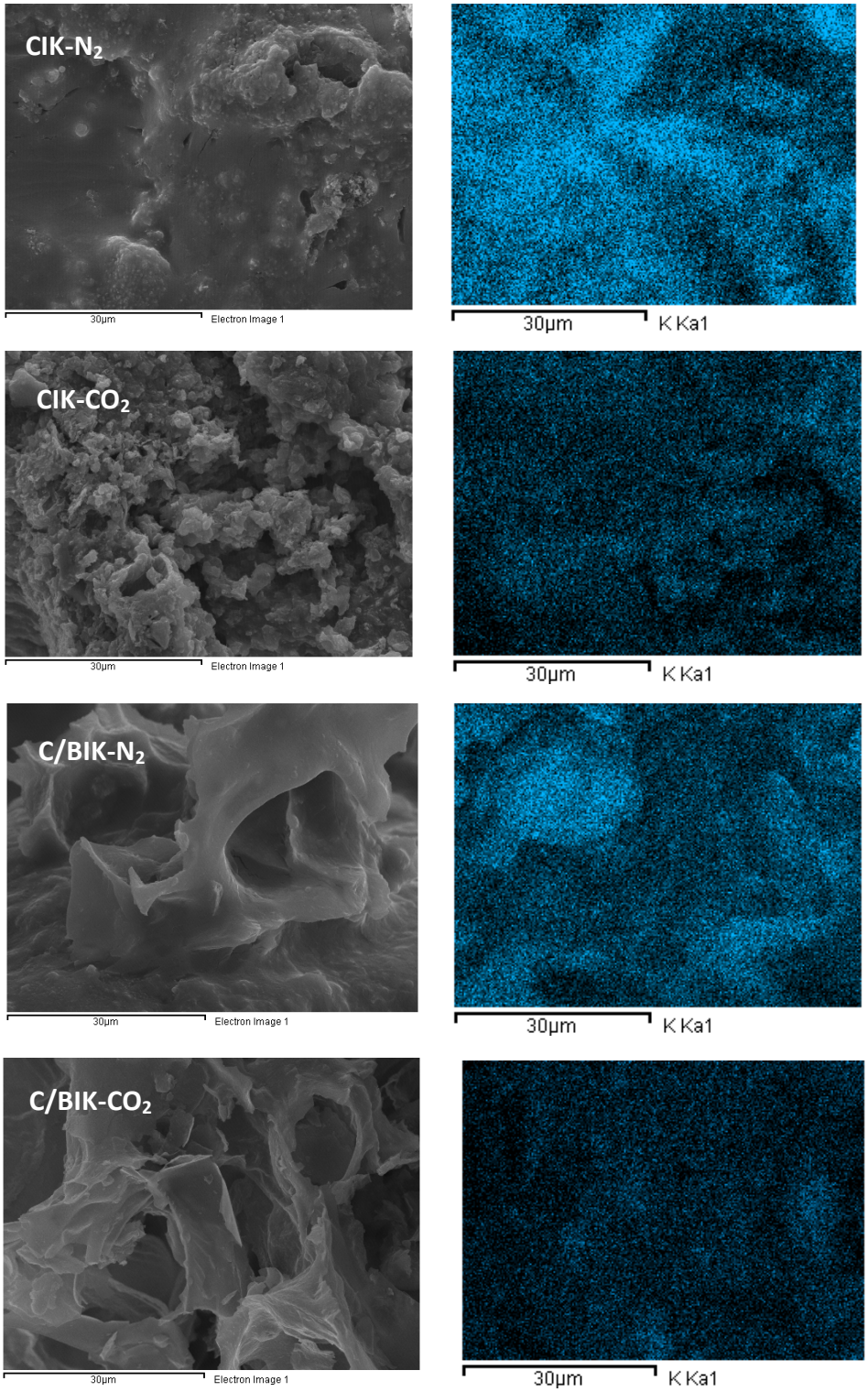

Figure 1. SEM-EDS mapping images of CIK and C/BIK chars obtained using N_2 or CO_2 at 600 °C

Table 2. BET surface and pore structure of non-impregnated chars

	B -CO_2	C-CO_2	C/B -CO_2	C/B-N_2
S_{BET} (m^2/g)	662	263	353	12
Total pore volume (cm^3/g)[a]	0.27	0.15	0.20	0.01
Micropore volume (cm^3/g)[a]	0.26	0.11	0.17	0.01
Micropore volume (cm^3/g)[b]	0.53	0.39	0.31	0.21

[a]Determined by N_2 physisorption. [b]Determined by CO_2 physisorption

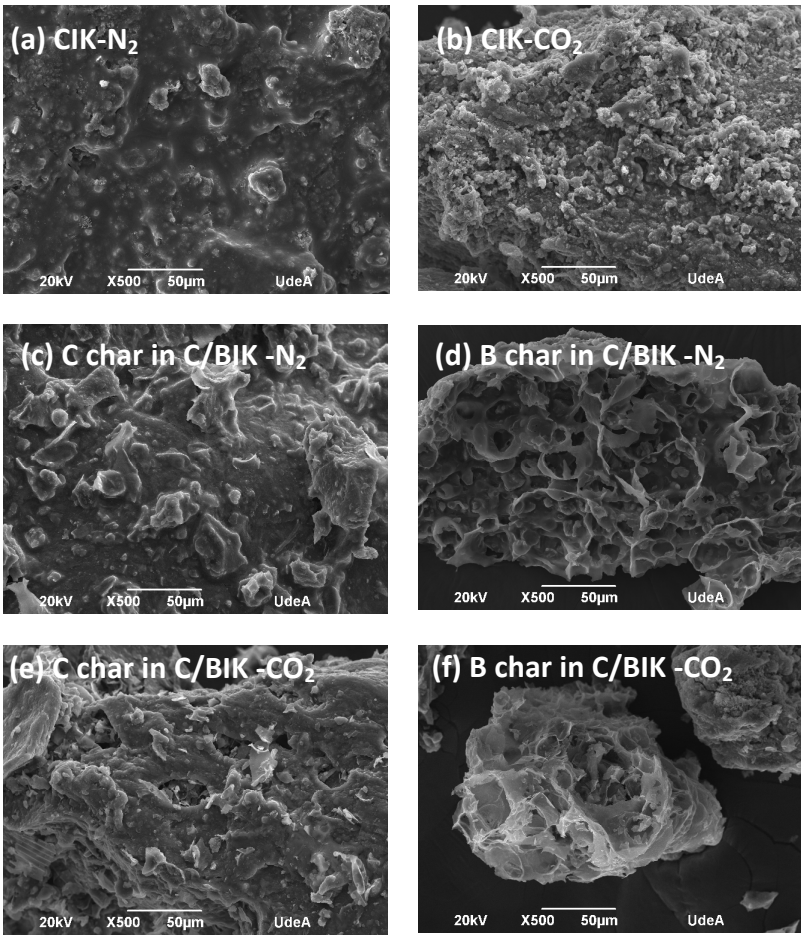

Figure 2. SEM images of CIK and C/BIK chars obtained under N_2 (a, c, d) and CO_2 (b, e, f) at 600 °C

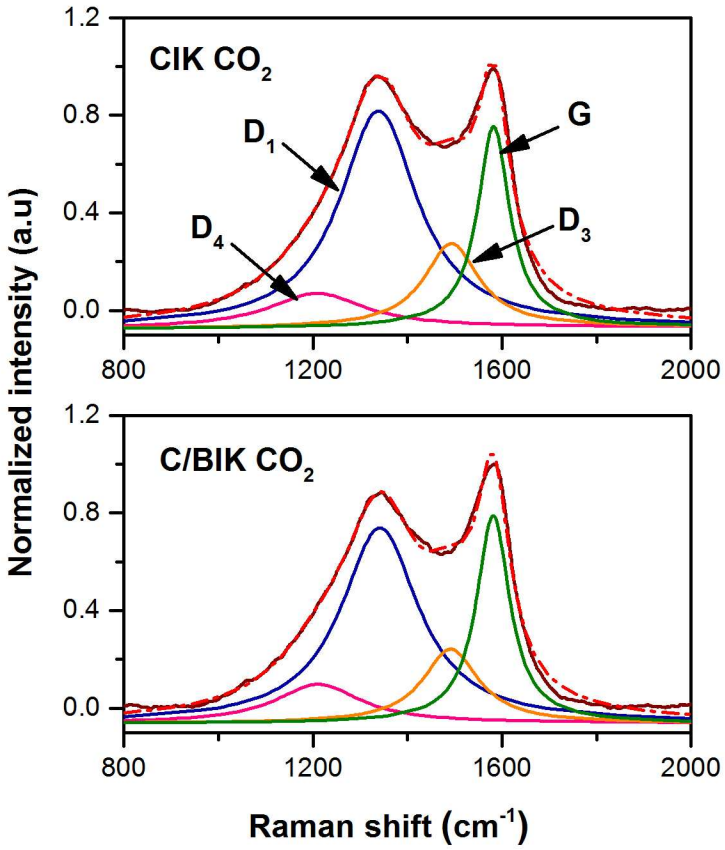

Figure 3. Raman spectra of CIK and C/BIK chars obtained under CO_2 atmosphere at 600 °C. Experimental data (-) and total fitted curve (---)

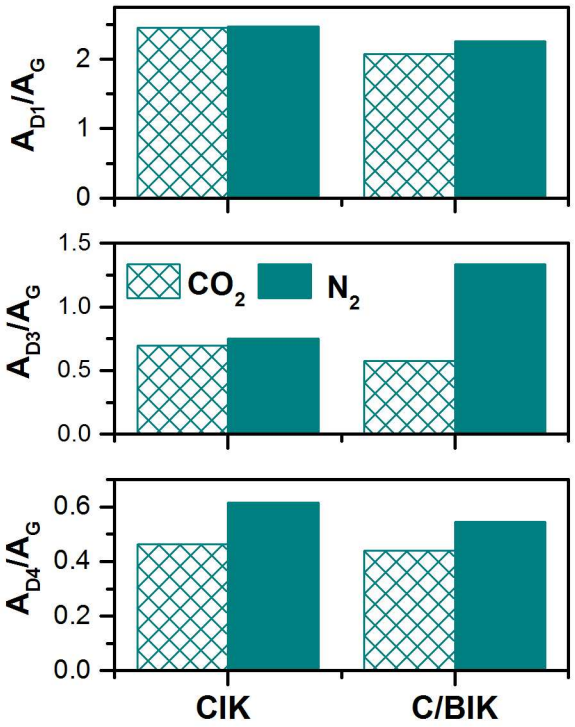

Figure 4. A_{Dx}/A_G ratio of the band peak areas of CIK and C/BIK chars prepared from CO_2 and N_2 atmosphere at 600 °C

Table 3. XPS-measured atomic surface composition in impregnated chars at 600 °C

Sample	Composition (%)		
	C1s	K2p	O1s
C/BIK-N_2	35.2	26.6	37.5
CIK-N_2	46.5	20.7	32.4
C/BIK-CO_2	52.4	18.4	27.9
CIK-CO_2	60.3	15.0	23.5

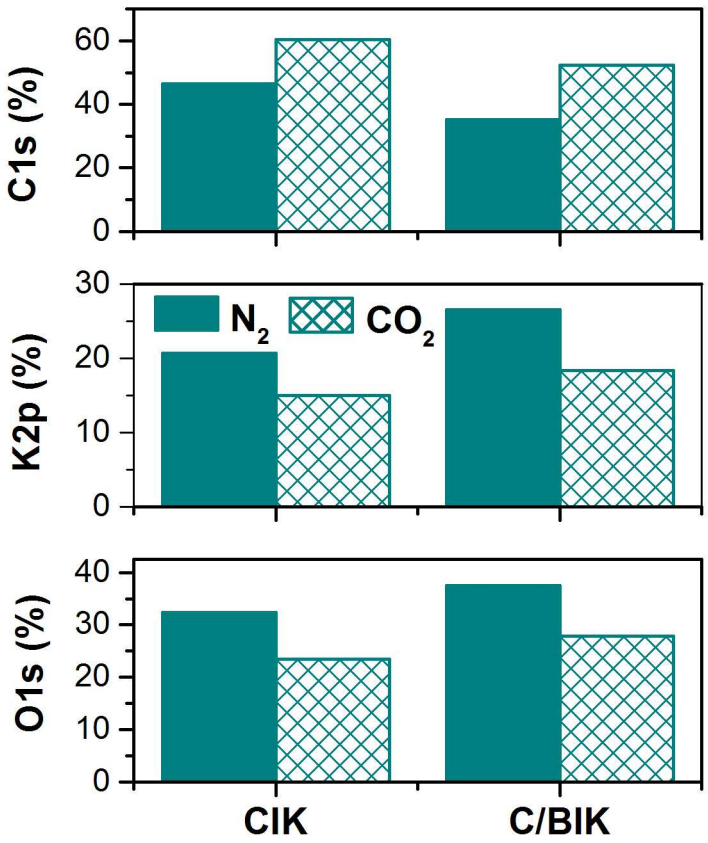

Figure 5. Comparative composition of the C1s, K2p and O1s species in the CIK and C/BIK chars obtained under N_2 and CO_2 atmospheres.

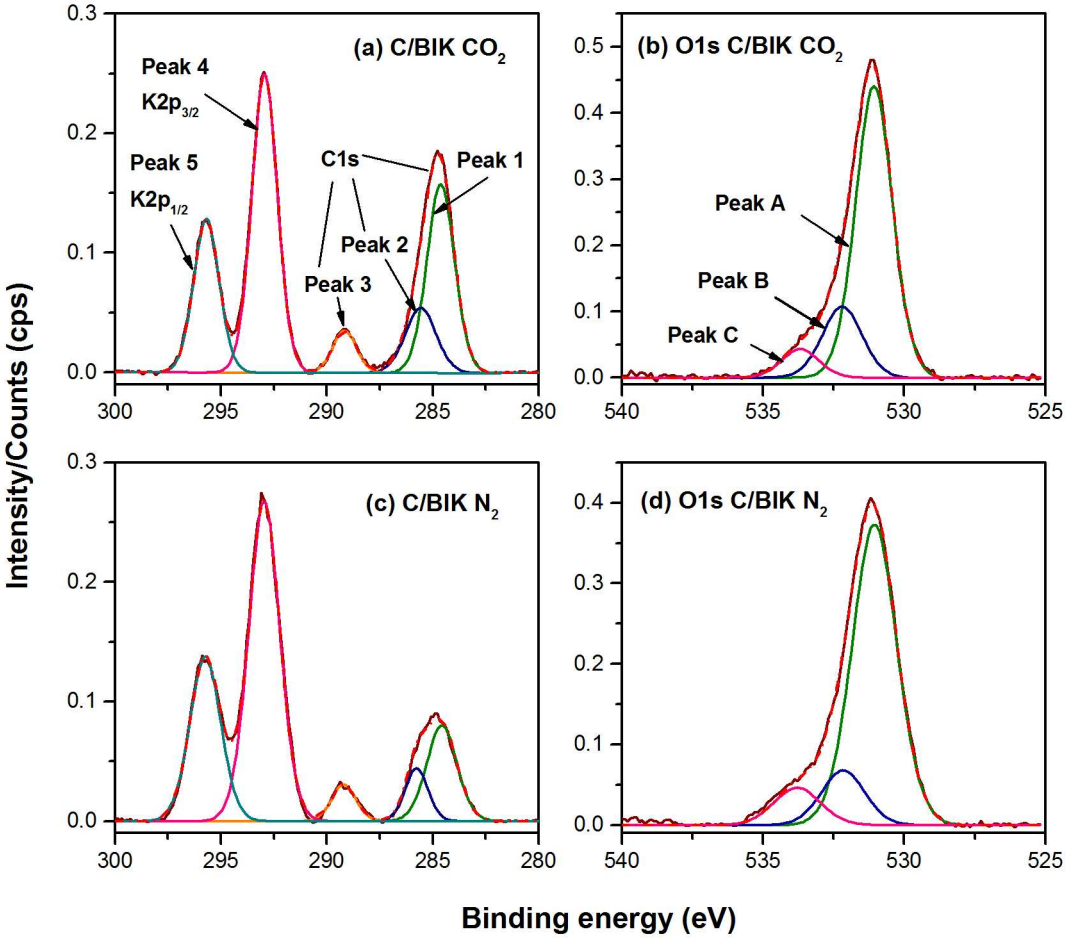

Figure 6. XPS spectra of C1s, K2p and O1s of C/BIK char using CO_2 (a-b) and N_2 (c-d)

Table 4. Areas of C1s and K2p species for impregnated chars under CO_2 and N_2

	C1s			K2p	
Binding energy (eV)	284.6	285.8	288.8	292.6	295.3
Sample	Peak 1	Peak 2	Peak 3	Peak 4	Peak 5
	C-C	C=O	O-C=O	K	K*
CIK -CO_2	39.0	6.7	4.7	32.8	16.8
CIK -N_2	26.1	4.8	5.2	42.1	21.8
C/BIK -CO_2	26.4	10.2	5.1	38.5	19.8
C/BIK -N_2	14.5	6.1	4.5	49.5	25.4

*Potassium associated with different functional groups [43].

Table 5. Area of O1s species for impregnated chars under CO_2 and N_2

	O1s		
Binding energy (eV)	531.6	533.2	534.9
Sample	Peak A	Peak B	Peak C
	C-O/C=O	C=O	C-O-C
CIK -CO_2	67.8	21.1	11.1
CIK -N_2	72.9	19.7	7.4
C/BIK -CO_2	73.3	19.3	7.4
C/BIK -N_2	76.5	13.5	10.0

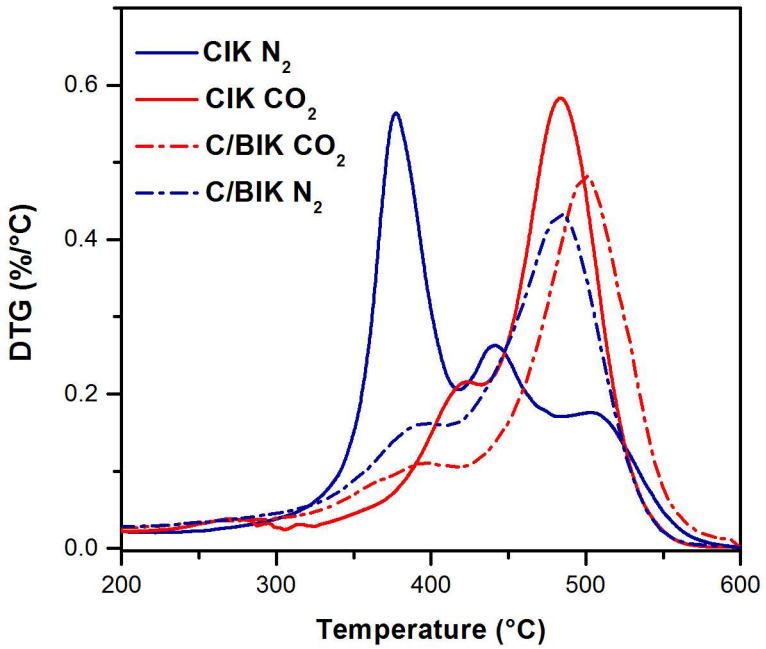

Figure 7. Oxy-combustion experiments performed with CIK and C/BIK prepared under N_2 and CO_2 at 600 °C. Oxy-combustion conditions: 21% O_2 + 79% CO_2 gas flow and heating rate of 5 °C/min

Table 6. Activation energy for CIK and C/BIK chars under oxy-combustion conditions

Sample	Ea (kJ/mol)
C/BIK-N_2	115
C/BIK-CO_2	141
CIK-N_2	85
CIK-CO_2	90

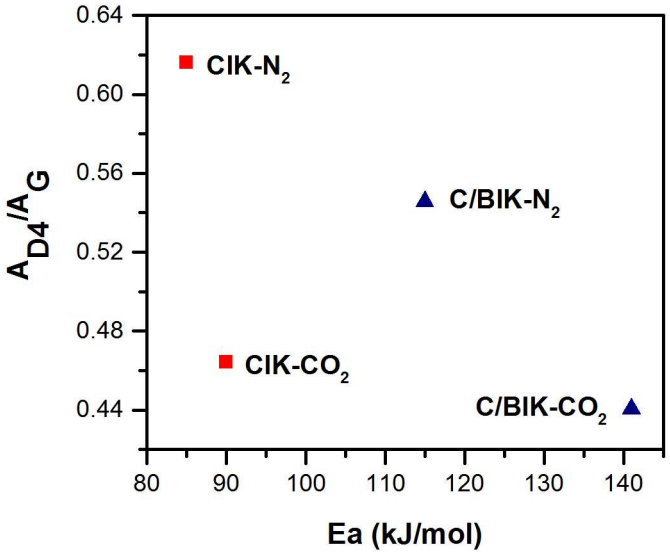

Figure 8. Correlation between the activation energies and active sites on the material surface of the CIK and C/BIK obtained under N_2 and CO_2 at 600 °C

Table 7. Monitored masses after $^{16}O_2/^{13}C^{18}O_2$ pulses over CIK and C/BIK chars

m/z	Specie	m/z	Specie
4	He	36	$^{18}O^{18}O$
18	$H_2O/^{18}O$	40	Ar
28	$^{12}C^{16}O$	44	$^{12}C^{16}O_2$
29	$^{13}C^{16}O$	45	$^{13}C^{16}O_2$
30	$^{12}C^{18}O$	46	$^{12}C^{16}O^{18}O$
31	$^{13}C^{18}O$	47	$^{13}C^{16}O^{18}O$
32	$^{16}O_2$	48	$^{12}C^{18}O_2$
34	$^{16}O^{18}O$	49	$^{13}C^{18}O_2$

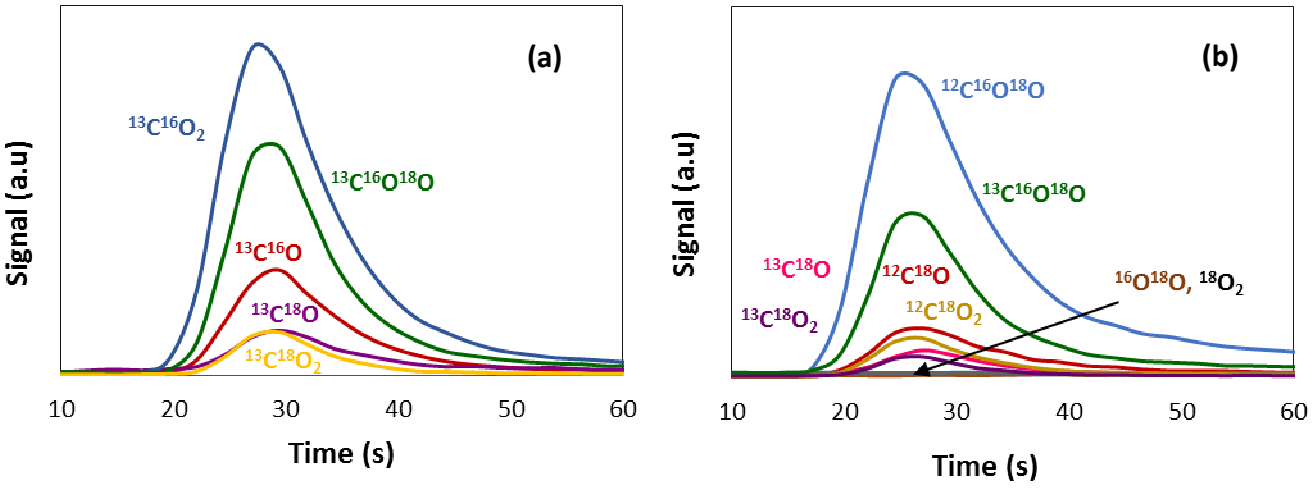

Figure 9. MS profiles monitored after $^{13}C^{18}O_2$ pulses to C/BIK CO_2 at 450 °C (a) ^{13}C carbon balance and (b) ^{18}O oxygen balance

Table 8. Percent of $^{12}C^{18}O$ evolution for impregnated and non-impregnated coal char, as a function of pre-treatment atmosphere and temperature

Sample	Temperature (°C)	% ($^{12}C^{18}O$)
C-N_2	450	13
	600	15
CIK-N_2	450	18
	600	21
C-CO_2	450	12
	600	14
CIK-CO_2	450	17
	600	20

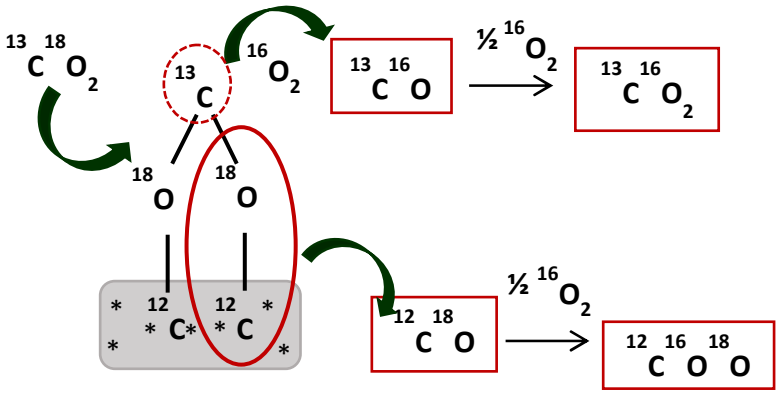

Figure 10. Molecular adsorption of $^{13}C^{18}O_2$ on two active sites, * represents the active sites associated with the K species presence

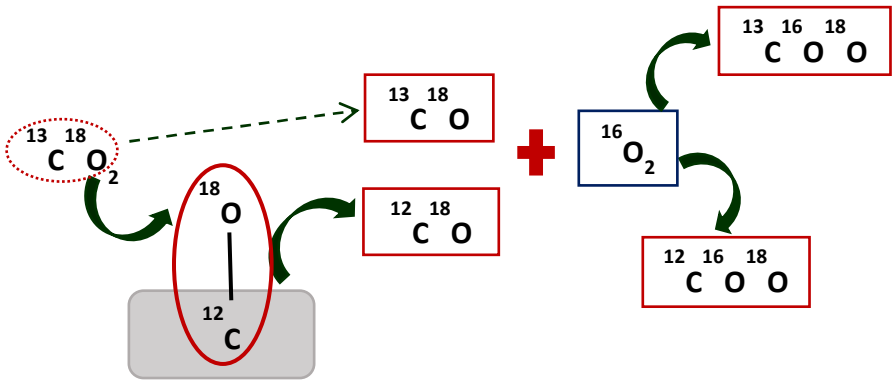

Figure 11. Dissociative adsorption of $^{13}C^{18}O_2$ on one active site